Journal of Porphyrins and Phthalocyanines
J. Porphyrins Phthalocyanines 2018; **22**: 542–551
DOI: 10.1142/S1088424618500529

Published at http://www.worldscinet.com/jpp/

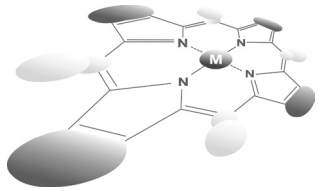

Redox switchable 19π and 18π 5,10,20-triaryl-5,15-diazaporphyrinoid–nickel(II) complexes

Keisuke Sudoh[a], Takuroh Hatakeyama[b], Ko Furukawa[c], Haruyuki Nakano[d] and Yoshihiro Matano*[,b◊]

[a]*Department of Fundamental Sciences, Graduate School of Science and Technology, Niigata University, Nishi-ku, Niigata 950-2181, Japan*
[b]*Department of Chemistry, Faculty of Science, Niigata University, Nishi-ku, Niigata 950-2181, Japan*
[c]*Center for Coordination of Research Facilities, Institute for Research Promotion, Niigata University, Nishi-ku, Niigata 950-2181, Japan*
[d]*Department of Chemistry, Graduate School of Science, Kyushu University, Fukuoka 819-0395, Japan*

Received 25 March 2018
Accepted 5 April 2018

ABSTRACT: The synthesis and optical, electrochemical, and magnetic properties of nickel(II) complexes of 5,10,20-triaryl-5,15-diazaporphyrin (TriADAP) are reported. Metal-templated cyclization of unsymmetrically substituted nickel(II)–bis(1-amino-9-chloro-5-mesityldipyrrin; mesityl = 2,4,6-trimethylphenyl) complexes afforded the corresponding TriADAPs or 5-aryl-15-benzyl-10,20-dimesityl-5,15-diazaporphyrin, depending on the combination of base and solvent. The latter macrocycle was converted to TriADAP by deprotection of the *N*-benzyl group through Pd/C-promoted hydrogenation. TriADAPs were isolated in both 18π (cation) and 19π (neutral) forms. The interconversion between these two oxidation states resulted in a distinct change in the optical properties of the DAP π-system. NMR spectroscopy of the 18π TriADAP cations showed that they had aromatic character, whereas EPR spectroscopy of the 19π TriADAP showed a highly delocalized electron spin of the π-radical. The *para* substituents of the *N*-aryl groups of TriADAPs had a small but distinct impact on their HOMO and LUMO energies. The change in the net charge of one electron was directly reflected in the redox properties of the DAP ring; TriADAP was more easily reduced and less easily oxidized than DAP. The difference in the net charge was also reflected by the shielding of the pyrrolic β-protons observed in the ^{1}H NMR spectra. The present results confirm that TriADAP is a highly promising framework for constructing a new class of azaporphyrin-based materials with 18π–19π redox-switchable optical and magnetic properties.

KEYWORDS: diazaporphyrin, redox property, aromaticity, radical.

INTRODUCTION

The redox properties of porphyrins are strongly associated with the aromatic, optical, and magnetic properties of the resulting oxidized/reduced macrocyclic π-systems [1–12]. The one-electron reduction of a 18π porphyrin ring produces a 19π radical anion, which is known to be an air-sensitive species because of its high-lying singly occupied molecular orbital (SOMO). Understanding of the fundamental properties of such radical species is important for both basic and applied research about redox catalysts and semiconducting materials. In 2015, Furuyama, Leznoff, Kobayashi and co-workers reported the first example of an extremely air-stable 19π porphyrinoid, a phosphorus(V) complex of 2,3,7,8,12,13,17,18-tetraaryl-5,10,15,20-tetraazaporphyrin [13]. Cyclic voltammetry and magnetic measurements showed this species to be a neutral π radical, and its remarkable stability was attributed to the electronic and steric effects of the central phosphorus(V) atom and bulky peripheral substituents. However, the

◊ SPP full member in good standing

*Correspondence to: Yoshihiro Matano, Department of Chemistry, Faculty of Science, Niigata University, Nishi-ku, Niigata 950-2181, Japan; tel.: +81-25-262-7734, fax: +81-25-262-7734, email: matano@chem.sc.niigata-u.ac.jp.

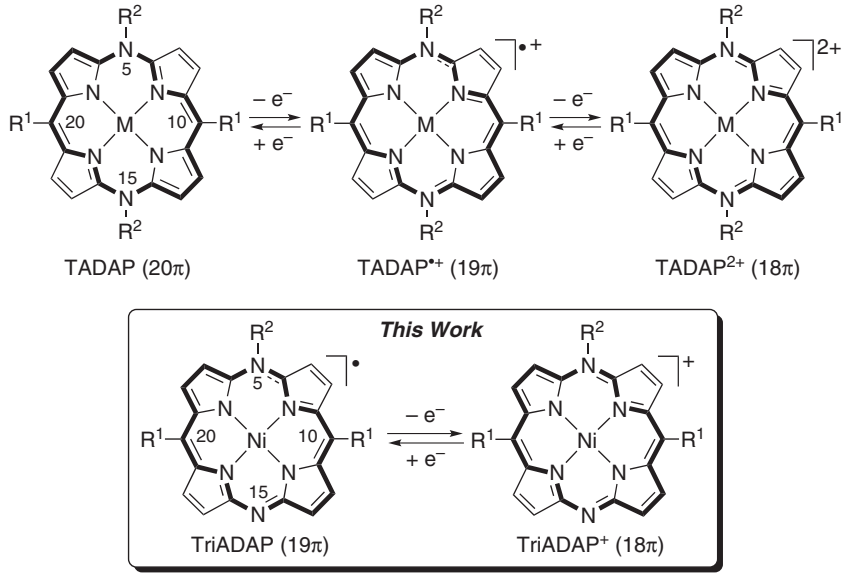

Chart 1. NiTADAP and NiTriADAP. R^1 = 2,4,6-$Me_3C_6H_2$; R^2 = aryl

number of air-stable 19π porphyrins is still limited, and structure–property/reactivity relationships of this class of compounds have not been comprehensively studied. Therefore, it is important to develop a conceptually new approach to obtaining porphyrin-based 19π-systems with excellent stability in air.

Recently, we reported the first examples of redox-switchable metal(II) complexes of 20π, 19π, and 18π 5,10,15,20-tetraaryl-5,15-diazaporphyrin (TADAP; Chart 1) [14, 15]. Incorporating the two nitrogen atoms at the 5 and 15-positions of a 5,10,15,20-tetraarylporphyrin (TAP) framework not only energetically stabilized the highest occupied molecular orbital (HOMO), lowest unoccupied molecular orbital (LUMO), and SOMO, but it also altered the net charge of the π-circuits of two electrons as a result of the electronic effects of two *meso* nitrogen atoms. Most importantly, these three π-systems can be handled in air. In particular, the 19π radical cations of TADAP were extremely stable towards dioxygen, moisture, and silica gel. We envisioned that this type of *meso*-C-to-N exchange strategy could be generally applied for the stabilization of unusual oxidation states of *meso*-arylated porphyrins and to make further advances in azaporphyrin-based redox materials. Herein, we report nickel(II) complexes of 5,10,20-triaryl-5,15-diazaporphyrin (TriADAP; Chart 1) as a new example of redox-switchable azaporphyrinoids. Our design concept for the synthesis of TriADAP was based on the idea that the replacement of two carbon atoms at the 5 and 15-positions of a 5,10,20-triarylporphyrin (TriAP) framework should alter the net charge of a single electron; the 19π-TriADAP, which is an isoelectronic form of the 19π TriAP radical anion, should be isolated in neutral form because unshared electron pairs on the *meso*-nitrogen atoms should be involved in the π-circuit. In this research, our aim was to establish a convenient method for the synthesis of TriADAP and to reveal the electronic effect of the net charge on the redox, aromatic, and optical properties of 5,15-diazaporphyrin (DAP) π-systems. As expected, TriADAPs reversibly interconverted between the neutral 19π and cationic 18π forms through single-electron transfer processes.

RESULTS AND DISCUSSION

First, we explored a modified protocol for the synthesis of 1-arylamino-9-chloro-5-mesityldipyrrins (mesityl = 2,4,6-trimethylphenyl) **1a**–**1d**, which were directly obtained by the reaction of 1,9-dichloro-5-mesityldipyrrin [16] with the corresponding anilines in acetonitrile (Scheme 1). This protocol enabled a gram-scale synthesis of **1a**–**1d** in a few steps from commercially available materials. Similarly, 1-benzylamino-9-chloro-5-mesityldipyrrin **2** was prepared in 97% yield from 1,9-dichloro-5-mesityldipyrrin and benzylamine. Treatment of nickel(II) acetate with an equimolar mixture of **1a** and **2** in MeOH gave unsymmetrically substituted nickel(II)–bis(dipyrrin) complex **3a** together with two kinds of symmetrically substituted nickel(II)–bis(dipyrrin) complexes **4a** and **5**. These three nickel(II) complexes were successfully separated by silica-gel column chromatography, and **3a** was isolated in 30% yield. The same procedure was used to prepare **3b**–**3d** in 40–46% yields from **1b**–**1d** and **2**.

Scheme 2 illustrates the synthesis of TriADAP by nickel-templated cyclization of **3a**. We used potassium carbonate and *N*,*N*-dimethylformamide (DMF) as base and solvent, respectively (method A), which were effective for the synthesis of 20π TADAP. Heating a DMF solution of **3a** in the presence of K_2CO_3 for 5 h at 110 °C afforded

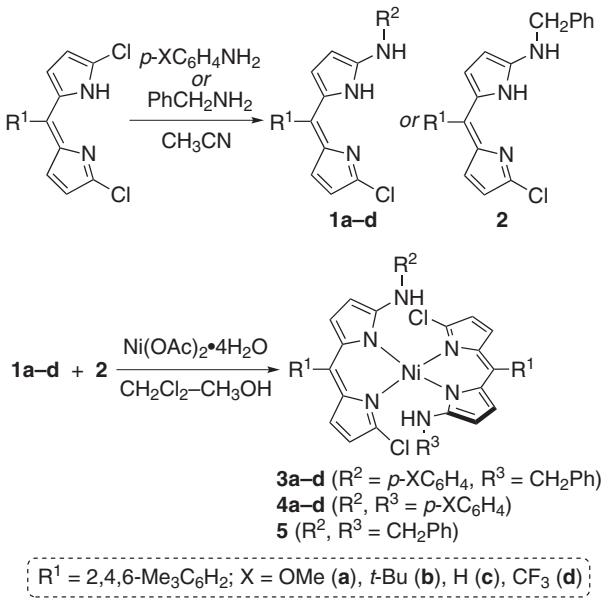

Scheme 1. Synthesis of **1**–**5**

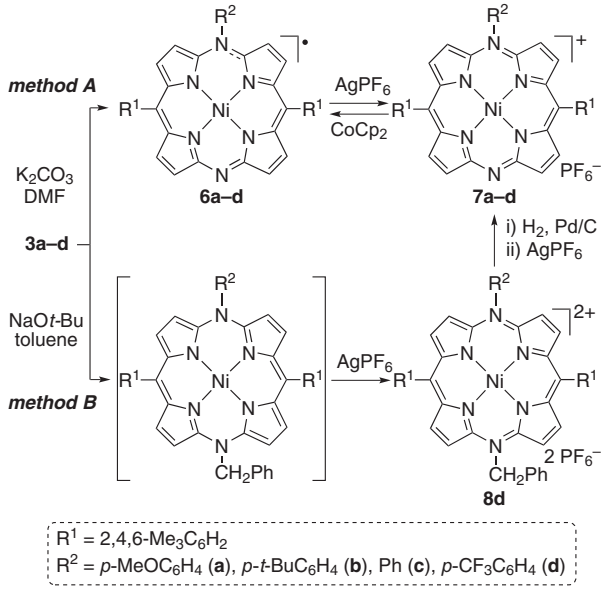

Scheme 2. Synthesis of **6**–**8**

19π TriADAP **6a** as a major cyclized product; however, the reaction mechanism for elimination of the *N*-benzyl group has not yet been clarified. Potassium hydroxide was also effective as a base for this annulation. It was difficult to isolate **6a** from the reaction mixture at this stage, so we converted **6a** to 18π TriADAP **7a** by *in situ* treatment with silver(I) hexafluorophosphate ($AgPF_6$). Cation **7a** was isolated as a purple solid by silica-gel column chromatography. Subsequently, a one-electron reduction of **7a** with cobaltocene ($CoCp_2$) proceeded cleanly to give **6a**, which was isolated as a greenish-yellow solid by recrystallization from MeOH. Method A was used to transform the other nickel(II)-bis(dipyrrin) complexes, **3b**–**3d**, to the corresponding 18π TriADAPs **7b**–**7d** *via* 19π TriADAPs **6b**–**6d**. The one-electron reduction of **7b**–**7d** afforded **6b**–**6d**. However, the yield of the *para*-trifluoromethyl-substituted derivative **7d** was not satisfactory (15%). Therefore, we examined another combination of base and solvent (NaO*t*-Bu and toluene) for the metal-templated cyclization of **3d**. Heating a toluene solution of **3d** in the presence of NaO*t*-Bu for 14 h at 110 °C followed by oxidation with two equivalents of $AgPF_6$ afforded the nickel(II) complex of 18π 5-aryl-15-benzyl-10,20-dimesityl-5,15-diazaporphyrin **8d** in dication form. Under these reaction conditions, the *N*-benzyl group was not cleaved. When exposed to dihydrogen gas in the presence of Pd/C, the *N*-benzyl group of **8d** was deprotected, and *in situ* oxidation of the resulting 20π species with $AgPF_6$ gave **7d** in 29% overall yield based on **3d**. Therefore, this two-step protocol (method B) was more effective than method A for the synthesis of **7d**.

The newly-prepared compounds were characterized by ^{1}H NMR and IR spectroscopy and high-resolution mass spectrometry (HRMS). In the HRMS data, intense molecular ion peaks ($[M]^+$) were observed for **6a**–**6d**, whereas fragment ion peaks consistent with $m/z = [M - PF_6]^+$ and $[M - 2(PF_6)]^{+\bullet}$ were detected for **7a**–**7d** and **8d**, respectively. In the IR spectra of **7a**–**7d**, a broad band owing to the P–F stretching vibration of the PF_6^- counterion was observed ($\nu = 843$–844 cm^{-1}). Considering that the one unshared electron pair on the *meso*-nitrogen atom at the 5-position is involved in the π-circuit, the 18π TriADAP cation is isoelectronic with 18π DAP.

As shown in Fig. 1a, the ^{1}H NMR spectrum of **7a** revealed a diatropic ring current by displaying strongly deshielded peaks owing to four kinds of β-protons at δ 8.38–9.22 ppm. The spectral features of **7a** clearly showed the aromatic character of its π-system. To determine the influence of the net charge as well as *N*-aryl substituents on the shielding effects of a DAP ring, the chemical shifts of the β-protons of **7a** were compared with those of 18π TADAP (R^1 = mesityl; R^2 = *p*-$MeOC_6H_4$) and 10,20-dimesityl-5,15-diazaporphyrin (DAP) (Figs. 1b and 1c). The chemical shifts of the β-protons at the 12,13,17,18-positions of **7a** (*c* and *d* in Fig. 1a) were similar to those of the corresponding protons of DAP (*a* and *b* in Fig. 1c) [17,18]. Conversely, the β-protons at the 2,3,7,8-positions of **7a** (*a* and *b* in Fig. 1a) were shifted slightly downfield compared with the corresponding protons of the TADAP dication (*a* and *b* in Fig. 1b), indicating that the net charge had an impact on the shielding effects of the DAP 18π-system.

A summary of the experimentally observed optical data for the TriADAPs and TADAPs is provided in Table 1. The ultraviolet/visible/near infrared (UV-vis/NIR) absorption spectra of **6a** and **7a** in CH_2Cl_2 are shown in Fig. 2. The 18π cation **7a** exhibited a low-energy

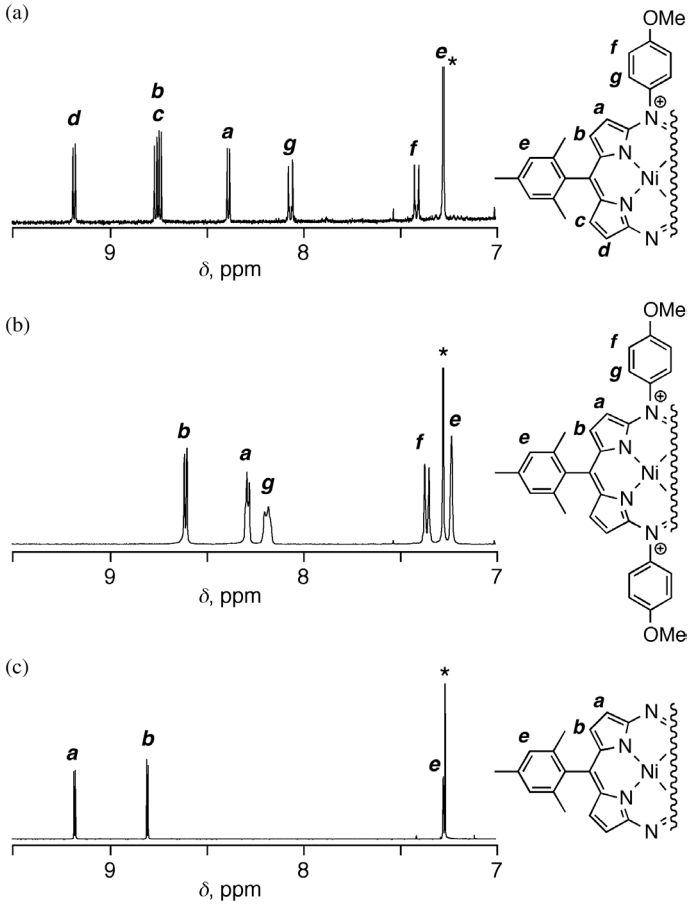

Fig. 1. ^{1}H NMR spectra (δ 7–9.5 ppm) of (a) **7a**, (b) NiTADAP, and (c) NiDAP in $CDCl_3$. Asterisks indicate residual solvent peak ($CHCl_3$)

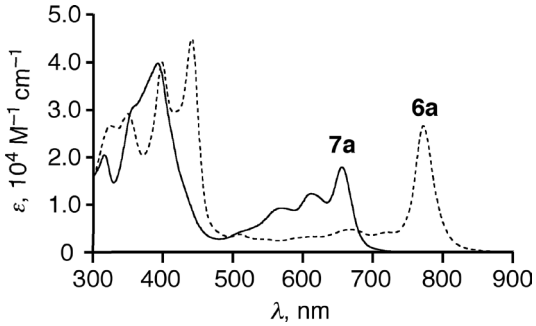

Fig. 2. UV-vis/NIR absorption spectra of **6a** (dotted line) and **7a** (solid line) in CH_2Cl_2

absorption band at a longer wavelength (λ_{max} = 655 nm) than 18π TADAP bearing the same *N*-substituents (λ_{max} = 629 nm), suggesting that the HOMO–LUMO gap of **7a** was slightly smaller than that of TADAP. Similar trends were observed for the absorption spectra of the other TriADAPs **7b**–**7d**. The longest-wavelength bands of **7a**–**7d** were red shifted compared with the Q bands of the β-unsubstituted DAP (λ_{max} = 571 nm) [17] and nickel(II) complex of 5,10,15-triphenylporphyrin (TPP) **9** (Fig. 3, λ_{max} = 554 nm) [19]. This indicated that the HOMO–LUMO gaps of the 18π TriADAPs were significantly smaller than those of the isoelectronic 18π DAP and TPP. Conversely, **6a**–**6d** exhibited an intense absorption band in the NIR region (λ_{max} = 772–777 nm), highlighting the characteristic optical properties of their 19π systems. In the series of TriADAP π-systems, the *para*-substituents of the *N*-aryl groups exerted only a small influence on the λ_{max} values.

To gain deeper insight into the nature of the π–π* electronic excitations of the TriADAP 18π-systems, we carried out time-dependent density functional theory (TD-DFT) calculations on **7-m** and reference porphyrin **9** (Fig. 3 and Table 2). In model **7-m**, the *meso*-mesityl groups were replaced by phenyl groups. Selected bond lengths and torsion angles (average values) of **7-m** and **9** are shown in Fig. 3. In the optimized structures, the bond lengths between the *meso*-N and α-C atoms (1.357, 1.315 Å) in **7-m** were considerably shorter than those between the *meso*-C and α-C atoms (1.393, 1.382 Å) in **9**. This bond shortening implied that the p orbitals of the *meso*-nitrogen atoms were effectively conjugated with the π-orbitals in the adjacent pyrrolic α carbon atoms in the TriADAP π-circuit. As shown in Fig. 3, both the HOMO/HOMO-1 and LUMO/LUMO+1 of **9** were almost degenerate, owing to the nearly D_{4h}-symmetric porphyrin π-system of **9**. In contrast, the corresponding orbitals of 18π

Table 1. Optical and electrochemical data for TriADAPs **6** and **7** and TADAPs[a]

	λ, nm[c]
6a	440 (4.65), 772 (4.42)
6b	440 (4.68), 772 (4.45)
6c	439, 773 (n.d.)
6d	438 (4.57), 777 (4.34)
7a	568 (3.96), 611 (4.09), 655 (4.25)
7b	567 (4.06), 611 (4.16), 656 (4.31)
7c	566 (4.01), 612 (4.12), 657 (4.29)
7d	566 (3.97), 617 (4.06), 663 (4.22)
8d	637 (4.43)
TADAP 20π[b]	446 (4.89), 531 (4.78)
TADAP 19π[b]	444 (4.78), 860 (4.47)
TADAP 18π[b]	444 (4.80), 629 (4.47)

[a]Measured in CH_2Cl_2. [b]Data from [15]. R^1 = 2,4,6-$Me_3C_6H_2$; R^2 = *p*-$MeOC_6H_4$. [c]Absorption maxima in the range of >400 nm. Data in parentheses are logarithms of extinction coefficients. N.d. = not determined.

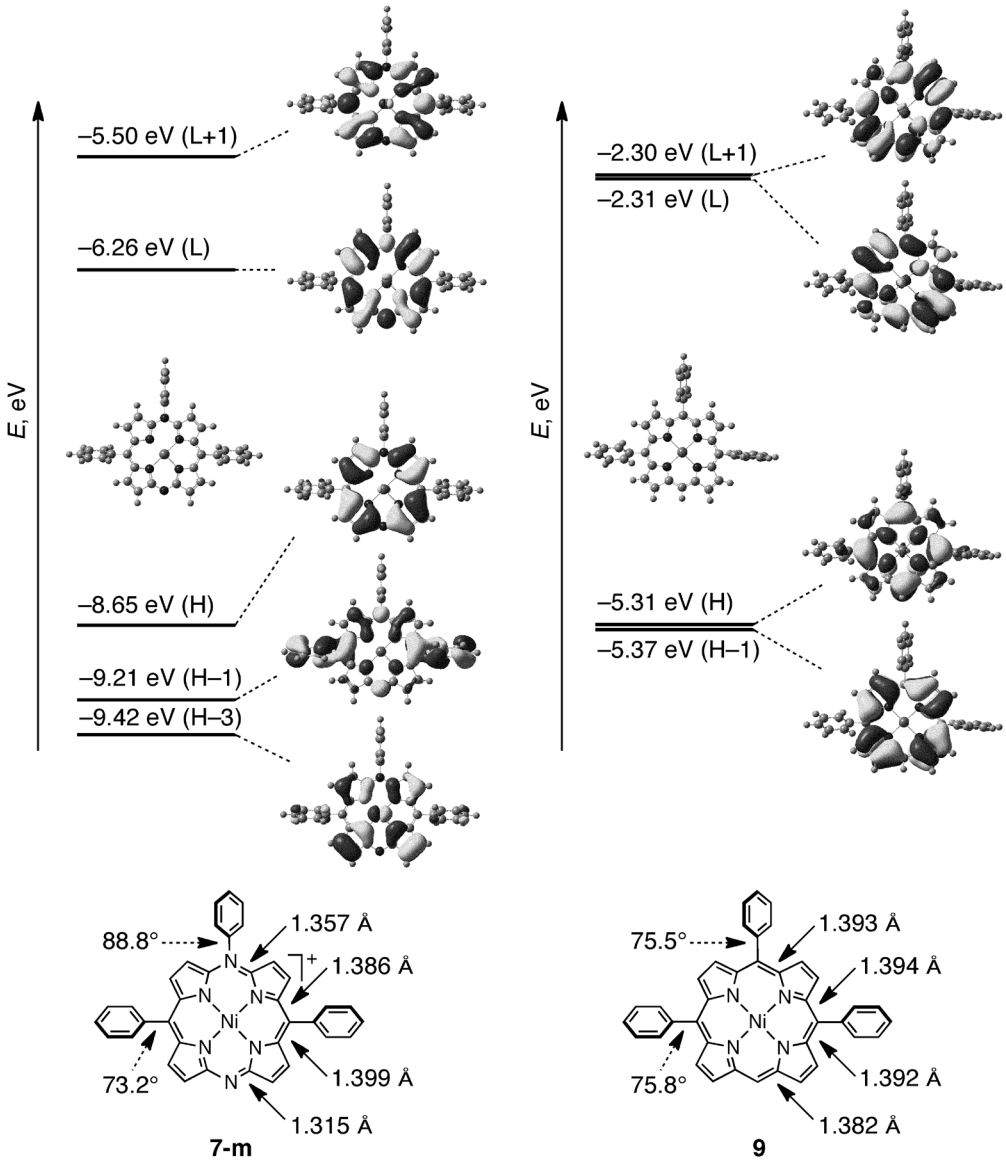

Fig. 3. Selected Kohn–Sham orbitals and their energies (in eV) of (a) **7-m** and (b) **9** calculated by the DFT method with the solvent effect (PCM, CH_2Cl_2). H = HOMO; L = LUMO. Selected bond lengths and dihedral angles (average values) are listed in the bottom

TriADAP cation **7-m** were nondegenerate because of the electronic influence of the *meso*-nitrogen atoms. The results of TD-DFT calculations suggested that the low-energy electronic transitions of **7-m** were basically composed of the HOMO-to-LUMO and HOMO−3-to-LUMO excitations, although the calculated excitation energies were not consistent with those observed for **7a**–**7d**.

Redox potentials of the TriADAPs were measured by cyclic voltammetry in CH_2Cl_2 with Bu_4NPF_6 as a supporting electrolyte. As shown in Fig. 4a, **7a**–**7d** exhibited three separate and reversible redox processes in the ranges −1.02 to −0.85 V, −0.39 to −0.32, and +1.41 to +1.47 V (*vs*. Ag/Ag^+), which were attributed to 20π/19π, 19π/18π, and 18π/17π redox processes, respectively. From these values, the electrochemical HOMO–LUMO gaps of the 18π TriADAP cations were determined to be 1.79–1.84 eV, which were in good agreement with the optical HOMO–LUMO gaps (*ca.* 1.8 eV) determined from their absorption spectra. The *para*-substituents of the *N*-aryl groups exerted small but clear effects on the HOMO and LUMO levels of the TriADAP π-systems (ΔE = −0.02 to −0.05 V for **7a** and +0.01 to +0.08 V for **7d** *vs*. **7c**). The electron-donating and electron-withdrawing effects of the *para*-substituents on TriADAP were comparable to those on TADAP [15]. As shown in Fig. 4b, the redox potentials of TriADAP were considerably shifted to the negative and positive sides, compared with the corresponding potentials of TADAP and DAP, respectively. These results clearly showed the effect of the net charge on the redox properties of the DAP π-system. The high air-stability of the neutral 19π radicals **6a**–**6d** probably stemmed from

Table 2. Excitation energies and oscillator strengths of **7-m** and **9** calculated by the TD-DFT method[a]

State	Excitation energy [eV/nm] (Oscillator strength)	Excitation (Weight [%])
7-m		
4	2.14/579 (0.234)	HOMO → LUMO (75.1), HOMO−3 → LUMO (18.0)
7	2.41/514 (0.143)	HOMO−3 → LUMO (75.4), HOMO → LUMO (18.0)
11	2.90/427 (0.117)	HOMO−8 → LUMO (55.7), HOMO → LUMO+1 (20.2)
18	3.21/387 (0.148)	HOMO−3 → LUMO+1 (66.0)
9		
4	2.389/519 (0.0004)	HOMO → LUMO+1 (43.0), HOMO−1 → LUMO (37.6)
5	2.391/519 (0.0027)	HOMO → LUMO (43.7), HOMO−1 → LUMO+1 (36.9)
12	3.15/393 (1.300)	HOMO−1 → LUMO (25.8), HOMO → LUMO+1 (21.8)
13	3.17/392 (0.854)	HOMO−1 → LUMO+1 (29.2), HOMO → LUMO (24.7)
14	3.18/390 (0.445)	HOMO−1 → LUMO+2 (47.6), HOMO−1 → LUMO (16.9)

[a] B3LYP/6-311G(d,p) and Wachters–Hay(f) (PCM, CH_2Cl_2) at the optimized structures. Except for the lowest-energy excited state of **9**, the states whose oscillator strengths are less than 0.1 are not included.

the positively shifted 19π/18π redox potentials of their π-systems compared with that of DAP.

Furthermore, we measured the EPR spectrum of **6d** in CH_2Cl_2 at room temperature. As shown in Fig. 5a, **6d** exhibited an EPR signal at $g = 2.0007$, which was successfully simulated with the fine structure derived from two *meso*-^{14}N, four inner-^{14}N, and eight β-^{1}H atoms. Because of the low symmetry of the TriADAP π-system, the spin densities on the two *meso*-N atoms were different. The calculated spin distribution of its model **6-m** supported the observed fine structure (Fig. 5b); the unshared electron spin of the 19π radical was efficiently delocalized over the entire DAP ring. This spin delocalization also played a key role in providing the high stability of the TriADAP 19π radical.

In summary, we prepared the first examples of 18π and 19π TriADAPs using metal-templated cyclization and redox reactions. In addition, the electronic effects of the *N*-aryl substituents on the optical and redox properties of the TriADAPs were studied using UV-vis/NIR absorption spectroscopy, cyclic voltammetry, and DFT calculations. Most importantly, neutral 19π radicals of TriADAP exhibited high stability to air, owing to the electronic effects of the *meso*-nitrogen atoms. The optical properties of TriADAPs varied considerably depending on the oxidation states of their π-systems. Furthermore, the 18π cations showed aromaticity in terms of the magnetic criterion, whereas the 19π radicals showed efficient delocalization of an unshared electron spin over the entire DAP ring. The results confirmed that replacing the two *meso*-carbon atoms of triarylporphyrins with nitrogen atoms is a promising strategy for constructing a new class of azaporphyrin-based materials with 18π–19π redox-switchable optical and magnetic properties.

EXPERIMENTAL

General

All melting points were recorded on a Yazawa micro melting point apparatus and are uncorrected. ^{1}H NMR spectra were recorded on an Agilent 700 MHz or 400 MHz spectrometer using $CDCl_3$ or CD_2Cl_2 as a solvent. Chemical shifts are reported as relative values *vs.* tetramethylsilane. High-resolution mass spectra (HRMS) were obtained on a Thermo Fisher Scientific EXACTIVE spectrometer. UV-vis absorption spectra were measured at room temperature on a JASCO V-530 spectrometer. IR spectra were measured on a PerkinElmer Spectrum GX spectrometer using KBr pellets. Electrochemical measurements were performed at room temperature on a CH Instruments model 650E electrochemical workstation using a glassy carbon working electrode, a platinum wire counter electrode, and an Ag/Ag^+ [0.01 M $AgNO_3$, 0.1 M Bu_4NPF_6 (MeCN)] reference electrode. The scan rate was 60 mV s^{-1}, and the potentials are reported *vs*. Ag/Ag^+. 1,9-Dichloro-5-mesityldipyrrin was

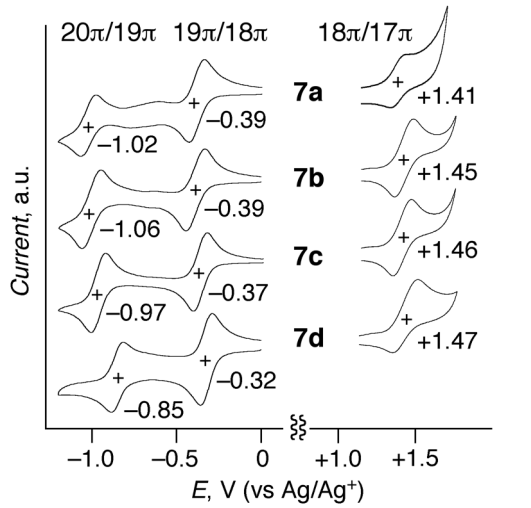

(a)

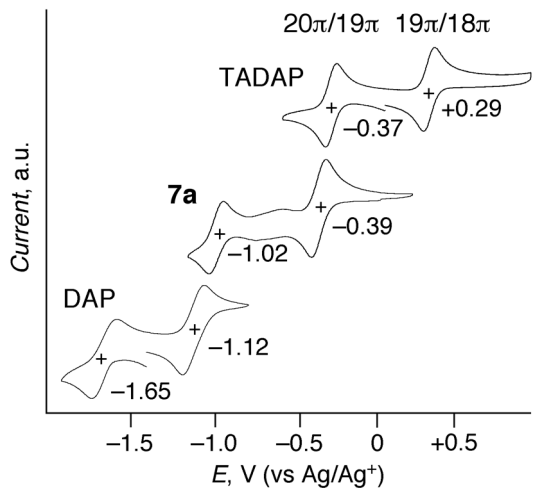

(b)

Fig. 4. Cyclic voltammograms and half-wave potentials of (a) **7a**–**7d** and (b) **7a**, TADAP, and DAP in CH_2Cl_2 with Bu_4NPF_6 as a supporting electrolyte

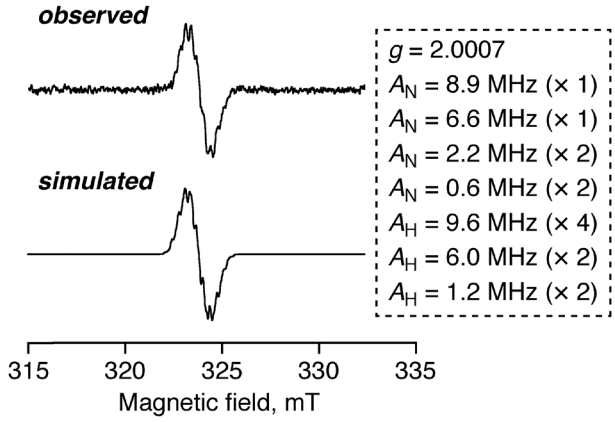

(a)

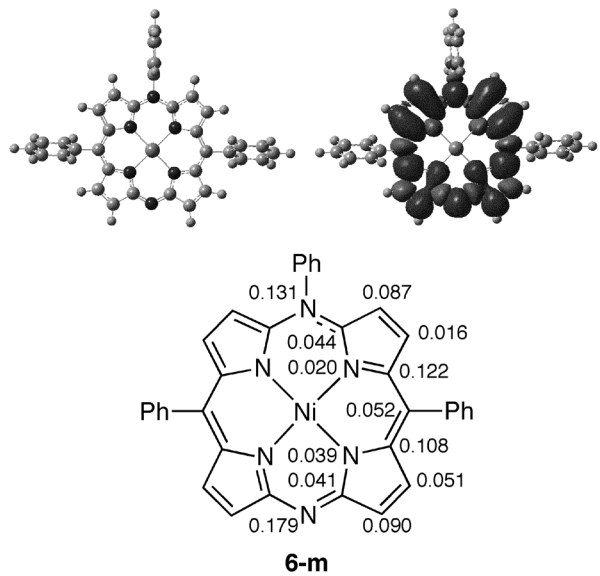

(b)

Fig. 5. (a) EPR spectra of **6d**: observed in CH_2Cl_2 at 298 K (upper) and simulated (lower). (b) Spin density distribution at the optimized structure (upper) and spin densities at the DAP ring (lower) of **6-m**; calculated by the DFT method with the solvent effect (PCM, CH_2Cl_2)

prepared according to the reported procedures [16]. Other chemicals and solvents were of reagent grade quality and used without further purification unless otherwise noted. Thin-layer chromatography was performed with Art. 5554 DC-Alufolien Kieselgel 60 F254 (Merck), and preparative column chromatography was performed using Silica Gel 60 spherical, neutral (Nacalai Tesque, Inc.). All reactions were performed under an argon or nitrogen atmosphere. The synthetic procedures and characterization data of new compounds are described below.

Synthesis and characterization

1-*Arylamino*-9-*chloro*-5-*mesityldipyrrins* (1a–1d). Typical procedure: a mixture of 1,9-dichloro-5-mesityldipyrromethene (1.840 g, 5.55 mmol), 4-methoxyaniline (1.717 g, 13.94 mmol), and MeCN (20 mL) was stirred for 18 h at room temperature. After being quenched with water, the aqueous layer was extracted with CH_2Cl_2, and the combined organic extracts were dried over Na_2SO_4 and evaporated under reduced pressure. The residue was then subjected to silica-gel column chromatography (hexane/AcOEt = 10/1). The red fraction (R_f = 0.53; hexane/AcOEt = 5/1) was collected and evaporated to give **1a** as a red oil (2.285 g, 98%). The other 1-arylamino-9-chloro-5-mesityldipyrrins **1b**–**1d** were similarly prepared from 1,9-dichloro-5-mesityldipyrromethene and the corresponding anilines. Compounds **1a**–**1d** were characterized by comparison with the reported spectral data.

1-*Benzylamino*-9-*chloro*-5-*mesityldipyrrin* (2). A mixture of 1,9-dichloro-5-mesityldipyrromethene (618 mg, 1.87 mmol), benzylamine (500 μL, 4.56 mmol), and MeCN (20 mL) was refluxed for 13 h. After being quenched with water, the aqueous layer was extracted with CH_2Cl_2, and the combined organic extracts were dried over Na_2SO_4 and evaporated under reduced pressure. The residue was then subjected to silica-gel column chromatography (hexane/AcOEt = 10/1). The red fraction (R_f = 0.42; hexane/AcOEt = 5/1) was collected and evaporated to give **2** as a red oil (729 mg, 97%).

2: ^{1}H NMR (400 MHz, $CDCl_3$): δ_H, ppm 2.11 (s, 6H, *ortho*-Me), 2.34 (s, 3H, *para*-Me), 4.73 (d, 2H, J = 4.8 Hz, CH_2), 5.05–5.12 (m, 1H, NH), 5.76 (d, 1H, J = 3.6 Hz, pyrrole-β), 5.95 (d, 1H, J = 3.6 Hz, pyrrole-β). 6.10 (d, 1H, J = 4.6 Hz, pyrrole-β), 6.52 (d, 1H, J = 4.6 Hz, pyrrole-β), 6.90 (s, 2H, Mes-*meta*), 7.32–7.35 (m, 1H, Ph), 7.36–7.45 (m, 2H, Ph), 7.46–7.50 (m, 2H, Ph) (one NH proton was not observed. probably due to the H/D exchange.); ^{13}C NMR (100 MHz, $CDCl_3$): δ_C, ppm 19.87, 20.94, 47.21, 107.94, 114.50, 118.24, 118.84, 125.29, 127.35, 127.62, 127.70, 128.58, 131.97, 132.80, 136.17, 136.74, 137.40, 138.39, 147.12, 165.90. HRMS (ESI): m/z calcd for $C_{25}H_{25}ClN_3$: 402.1732, $[M + H]^+$; found: 402.1720; R_f = 0.42 (hexane/AcOEt = 5/1).

***Nickel*(II)–*bis*(*dipyrrin*) *complexes* (3a–3d, 4a–4d, *and* 5).** Typical procedure: a mixture of **1a** (202 mg, 0.48 mmol), **2** (197 mg, 0.49 mmol), $Ni(OAc)_2 \cdot 4H_2O$ (132 mg, 0.53 mmol), triethylamine (1 mL), CH_2Cl_2 (10 mL), and MeOH (10 mL) was stirred for 16 h at room temperature. The mixture was concentrated under reduced pressure. The residue was then subjected to silica-gel column chromatography (hexane/AcOEt = 10/1). TLC indicated three fractions (R_f = 0.52, 0.59, 0.65; hexane/AcOEt = 5/1), of which the second fraction (R_f = 0.59) was collected, concentrated, and recrystallized from MeOH to give **3a** as a reddish-brown solid (127 mg, 30%). The other fractions were also collected and recrystallized. The first (R_f = 0.65) and third (R_f = 0.52) fractions were evaporated to give **5** (42 mg, 10%) and **4a** (128 mg, 29%), respectively, as reddish-brown solids. Compounds **3b**–**3d** were similarly prepared in 40–46% yields from **1b**–**1d** and **2**. Compounds **4a**–**4c** were characterized by comparison with the reported spectral data [15].

3a (R_f = 0.59; hexane/AcOEt = 5/1). Reddish-brown solid, mp 184–186 °C. HRMS (ESI): m/z 875.2531 ($[M + H]^+$) (calcd for $C_{50}H_{47}Cl_2N_6ONi$ 875.2536).

3b (R_f = 0.64; hexane/AcOEt = 5/1). Reddish-brown solid, mp 165–168 °C. HRMS (ESI): m/z 900.2985 ($[M]^+$) (calcd for $C_{53}H_{52}Cl_2N_6Ni$: 900.2979). Yield 46%.

3c (R_f = 0.63; hexane/AcOEt = 5/1). Reddish-brown solid, mp 186 °C. HRMS (ESI): m/z 844.2353 ($[M]^+$) (calcd for $C_{49}H_{44}Cl_2N_6Ni$: 844.2344). Yield 40%.

3d (R_f = 0.59; hexane/AcOEt = 5/1). Reddish-brown solid, mp 190–191 °C. HRMS (ESI): m/z 912.2219 ($[M + H]^+$) (calcd for $C_{50}H_{43}Cl_2F_3N_6Ni$: 912.2226). Yield 40%.

4d (R_f = 0.52; hexane/AcOEt = 5/1). Reddish-brown solid, mp 196–198 °C. HRMS (ESI): m/z 966.1926 ($[M]^+$) (calcd for $C_{50}H_{40}Cl_2F_6N_6Ni$: 966.1944).

5 (R_f = 0.65; hexane/AcOEt = 5/1). Reddish-brown solid, mp 179–180 °C. HRMS (ESI): m/z 859.2565 ($[M + H]^+$) (calcd for $C_{50}H_{47}Cl_2N_6Ni$: 859.2587).

18π *Nickel*(II) *Complexes of* 5,10,20-*Triaryl*-5,15-*diazaporphyrin* (7a–7d). These compounds were prepared by two different methods.

Method A. A mixture of **3a** (95.4 mg, 0.11 mmol), K_2CO_3 (54.2 mg, 0.40 mmol), and DMF (50 mL) was stirred for 5 h at 110 °C. After being quenched with water, the aqueous layer was extracted with toluene, and the combined organic extracts were washed with brine, dried over Na_2SO_4, and evaporated under reduced pressure. UV-vis/NIR absorption spectroscopy and HRMS spectrometry of the residue showed the formation of **6a**. As it was difficult to isolate **6a** at this stage, the residue was dissolved in CH_2Cl_2, and $AgPF_6$ (42 mg, 0.16 mmol) was added to the solution. The resulting mixture was stirred for 2 min at room temperature and then filtered through a Celite bed. The filtrate was concentrated under reduced pressure to leave a solid residue, which was then subjected to silica-gel column chromatography (CH_2Cl_2/Acetone = 40/1). The blue fraction (R_f = 0.56; CH_2Cl_2/Acetone = 20/1) was collected, concentrated and recrystallized from CH_2Cl_2–hexane to give **7a** as a purple solid (25.2 mg, 27%). Compounds **7b**–**7d** were similarly prepared in 15–33% yields from **3b**–**3d**. When KOH was used instead of K_2CO_3, **3a** was obtained in 10% yield.

Method B. A mixture of **3d** (40.0 mg, 0.044 mmol), *t*-BuONa (21.5 mg, 0.22 mmol), and toluene (15 mL) was stirred for 14 h at 110 °C. After quenching with water, the aqueous layer was extracted with toluene, and the combined organic extracts were washed with brine, dried over Na_2SO_4, and evaporated under reduced pressure. The formation of 20π species (shown in a bracket of Scheme 2) was confirmed by thin-layer chromatography. The residue was dissolved in CH_2Cl_2, and $AgPF_6$ (27.8 mg, 0.11 mmol) was added to the solution. The resulting mixture was stirred for 2 min at room temperature and then passed through a Celite bed. The eluent was concentrated under reduced pressure and recrystallized from CH_2Cl_2–hexane to give **8d** as a green solid (32.0 mg, 72%).

A MeOH solution of **8d** (141.6 mg, 0.13 mmol) was stirred under hydrogen atmosphere in the presence of Pd/C (10 mg, 1 mol%) for 8 days and then passed through a Celite bed. The eluent was concentrated under reduced pressure, and water was added. The aqueous layer was extracted with CH_2Cl_2, and the combined organic extracts were washed with brine, dried over Na_2SO_4, and evaporated under reduced pressure. The residue was dissolved in CH_2Cl_2, and $AgPF_6$ (41.4 mg, 0.16 mmol) was added to the solution. The resulting mixture was stirred for 2 min at room temperature, and then passed through a Celite bed. The eluent was concentrated under

reduced pressure, and the residue was then subjected to silica-gel column chromatography (CH_2Cl_2/MeOH = 20/1). The blue fraction (R_f = 0.43; CH_2Cl_2/MeOH = 20/1) was collected, concentrated, and recrystallized from CH_2Cl_2–hexane to give **7d** as a purple solid (45.0 mg, 40%).

7a (R_f = 0.56; CH_2Cl_2/MeOH = 20/1): Purple solid, mp 210–213 °C; ^{1}H NMR (700 MHz, CD_2Cl_2): δ_H, ppm 1.81 (s, 12H, *ortho*-Me), 2.59 (s, 6H, *para*-Me), 4.10 (s, 3H, OMe), 7.31 (s, 4H, Mes-*meta*), 7.40 (d, 2H, *J* = 8.4 Hz, Ar), 7.96 (d, 2H, *J* = 8.4 Hz, Ar), 8.38 (d, 2H, *J* = 5.2 Hz, pyrrole-β), 8.76 (d, 2H, *J* = 4.2 Hz, pyrrole-β), 8.80 (d, 2H, *J* = 5.2 Hz, pyrrole-β), 9.22 (d, 2H, *J* = 4.2 Hz, pyrrole-β), IR (KBr): ν, cm^{-1} 843 (PF_6^-). HRMS (ESI): *m*/*z* 711.2361 ([*M* – PF_6]$^+$) (calcd for $C_{43}H_{37}N_6ONi$: 711.2377). UV-vis (CH_2Cl_2): λ_{max}, nm (log ε) 391 (4.60), 568 (3.96), 611 (4.09), 655 (4.25).

7b (R_f = 0.25; CH_2Cl_2/MeOH = 20/1): Purple solid, mp 239–241 °C. ^{1}H NMR (700 MHz, CD_2Cl_2): δ_H, ppm 1.59 (s, 9H, *t*Bu), 1.81 (s, 12H, *ortho*-Me), 2.59 (s, 6H, *para*-Me), 7.31 (s, 4H, Mes-*meta*), 7.94 (d, 2H, *J* = 8.8 Hz, Ph), 7.98 (d, 2H, *J* = 8.8 Hz, Ph), 8.35 (d, 2H, *J* = 5.2 Hz, pyrrole-β), 8.76 (d, 2H, *J* = 4.2 Hz, pyrrole-β), 8.80 (d, 2H, *J* = 5.2 Hz, pyrrole-β), 9.22 (d, 2H, *J* = 4.2 Hz, pyrrole-β), IR (KBr): ν, cm^{-1} 843 (PF_6^-). HRMS (ESI): *m*/*z* 737.2890 ([*M* – PF_6]$^+$) (calcd for $C_{46}H_{43}N_6Ni$: 737.2897). UV-vis (CH_2Cl_2): λ_{max}, nm (log ε) 392 (4.69), 567 (4.06) 611 (4.16) 656 (4.31).

7c (R_f = 0.38; CH_2Cl_2/MeOH = 20/1): Purple solid, mp 221 °C. ^{1}H NMR (700 MHz, CD_2Cl_2): δ_H, ppm 1.80 (s, 12 H, *ortho*-Me), 2.58 (s, 6H, *para*-Me), 7.30 (s, 4H, Mes-*meta*), 7.93–7.97 (m, 2H, Ph), 8.05–8.09 (m, 3H, Ph), 8.30 (d, 2H, *J* = 4.9 Hz, pyrrole-β), 8.76 (d, 2H, *J* = 4.9 Hz, pyrrole-β), 8.79 (d, 2H, *J* = 4.9 Hz, pyrrole-β) 9.21 (d, 2H, *J* = 4.9 Hz, pyrrole-β). IR (KBr): ν, cm^{-1} 843 (PF_6^-). HRMS (ESI): *m*/*z* 681.2264 ([*M* – PF_6]$^+$) (calcd for $C_{42}H_{35}N_6Ni$: 681.2271). UV-vis (CH_2Cl_2): λ_{max}, nm (log ε) 392 (4.66), 566 (4.01), 612 (4.12), 657 (4.29).

7d (R_f = 0.43; CH_2Cl_2/MeOH = 20/1): Purple solid, mp 226–227 °C. ^{1}H NMR (700 MHz, CD_2Cl_2): δ_H, ppm 1.81 (s, 12H, *ortho*-Me), 2.59 (s, 6H, *para*-Me), 7.31 (s, 4H, Mes-*meta*), 8.25 (s, 4H, Ar), 8.26 (d, 2H, *J* = 4.9 Hz, pyrrole-β), 8.77 (d, 2H, *J* = 4.9 Hz, pyrrole-β), 8.83 (d, 2H, *J* = 4.9 Hz, pyrrole-β), 9.23 (d, 2H, *J* = 4.9 Hz, pyrrole-β). IR (KBr): ν, cm^{-1} 844 (PF_6^-). HRMS (ESI): *m*/*z* 749.2130 ([*M* – PF_6]$^+$) (calcd for $C_{43}H_{34}N_6F_3Ni$: 749.2145). UV-vis (CH_2Cl_2): λ_{max}, nm (log ε) 391 (4.60), 566 (3.97) 617 (4.06) 663 (4.22).

8d (R_f = 0.47; CH_2Cl_2/MeOH = 20/1), mp 173–175 °C. ^{1}H NMR (400 MHz, $CDCl_3$): δ_H, ppm 1.85 (s, 12H, *ortho*-Me), 2.53 (s, 6H, *para*-Me), 7.20 (s, 4H, Mes-*meta*), 7.36 (s, 2H, C*H*$_2$Ph), 7.47–7.53 (m, 5H, Ar), 8.18 (d, 2H, *J* = 8.2 Hz, $CF_3C_6H_4$), 8.27 (d, 2H, *J* = 5.2 Hz, pyrrole-β), 8.44 (d, 2H, *J* = 8.2 Hz, $CF_3C_6H_4$), 8.70 (d, 2H, *J* = 5.2 Hz, pyrrole-β), 8.78 (d, 2H, *J* = 5.2 Hz, pyrrole-β), 9.11 (d, 2H, *J* = 5.2 Hz, pyrrole-β). HRMS (ESI): *m*/*z* 840.2683 ([*M* – 2PF_6]$^+$) (calcd for $C_{50}H_{41}F_3N_6Ni$: 840.2693). UV-vis (CH_2Cl_2): λ_{max}, nm (log ε) 335 (4.52), 396 (4.80), 637 (4.44).

19π *Nickel*(II) *Complexes of* 5,10,20-*Triaryl*-5,15-*diazaporphyrin* (6a–6d). A mixture of **7a** (9.2 mg, 11 μmol), cobaltocene (3.2 mg, 17 μmol), and THF (10 mL) was stirred for 2 min at room temperature. The mixture was concentrated under reduced pressure. The residue was dissolved in hexane and filtrated through a Celite bed several times. The filtrate was then concentrated under reduced pressure and recrystallized from MeOH to give **6a** as a greenish-yellow solid (1.6 mg, 21%). Compounds **6b**–**6d** were similarly prepared in 20–33% yields from **7b**–**7d**.

6a (R_f = 0.48; CH_2Cl_2/MeOH = 20/1): Greenish-yellow solid, mp >300 °C. HRMS (ESI): *m*/*z* 711.2355 ([*M*]$^+$) (calcd for $C_{43}H_{37}N_6ONi$: 711.2377). UV-vis (CH_2Cl_2): λ_{max}, nm (log ε) 323 (4.42), 348 (4.46), 397 (4.60), 440 (4.65), 772 (4.42).

6b (R_f = 0.38; CH_2Cl_2/MeOH = 20/1): Greenish-yellow solid, mp >300 °C. HRMS (ESI): *m*/*z* 737.2898 ([*M*]$^+$) (calcd for $C_{46}H_{43}N_6Ni$: 737.2897). UV-vis (CH_2Cl_2): λ_{max}, nm (log ε) 322 (4.46), 348 (4.49), 397 (4.64), 440 (4.68), 772 (4.45).

6c (R_f = 0.43; CH_2Cl_2/MeOH = 20/1): Greenish-yellow solid, mp >300°C. HRMS (ESI): *m*/*z* 681.2270 ([*M*]$^+$) (calcd for $C_{42}H_{35}N_6Ni$: 681.2271). UV-vis (CH_2Cl_2): λ_{max}, nm 323, 347, 396, 439, 773.

6d (R_f = 0.70; CH_2Cl_2/MeOH = 20/1): Greenish-yellow solid, mp >300 °C. HRMS (ESI): *m*/*z* 749.2148 ([*M*]$^+$) (calcd for $C_{43}H_{34}N_6F_3Ni$: 749.2145). UV-vis (CH_2Cl_2): λ_{max}, nm (log ε) 322 (4.34), 346 (4.35), 396 (4.50), 438 (4.57), 777 (4.34).

Computational details

The geometries of the model compounds were optimized using the DFT method. The basis sets used were the 6-311G(d,p) basis set [20] for H, C, and N and the Wachters–Hay all electron basis set [21] supplemented with one *f*-function (exponent: 1.29) for Ni. The functional of DFT was the Becke, three-parameter, Lee–Yang–Parr (B3LYP) exchange–correlation functional [22]. We confirmed that the optimized geometries were not in saddle but in stable points. All the calculations were carried out using the Gaussian 09 suite of programs [23].

EPR measurements

The electron paramagnetic resonance (EPR) spectrum of 19π Ni^{II}TADAP 6a was measured at room temperature by using a JEOL JES-FA200 spectrometer equipped with an OXFORD ESR900 He-flow cryostat. The sample was prepared as a 0.1 mM solution in CH_2Cl_2. After three freeze-pump-thaw cycles, the solution sample in a quartz tube was sealed by frame. Spectral simulation was performed using EasySpin [24], which is a MATLAB toolbox designed for this. The static magnetic field and microwave frequency were measured by Echo

Electronics EFM-2000 gauss meter and TakedaRiken TR5212 microwave counters, respectively.

Acknowledgments

This work was supported by JSPS KAKENHI (Grant Numbers: 15K13762 to YM, 15K05392 to HN) and Union Tool Foundation.

REFERENCES

1. Kadish KM, Van Caemelbecke E and Royal G. In *The Porphyrin Handbook,* Vol. 8. Kadish KM, Smith KM and Guilard R. (Eds.) Academic Press: San Diego, CA, 2000; pp. 1–114.
2. Reddy BK, Basavarajappa A, Ambhore MD and Anand VG. *Chem. Rev.* 2017; **117**: 3420–3443.
3. Yamamoto Y, Yamamoto A, Furuta S, Horie M, Kodama M, Sato W, Akiba K, Tsuzuki S, Uchimaru T, Hashizume D and Iwasaki F. *J. Am. Chem. Soc.* 2005; **127**: 14540–14541.
4. Cissell JA, Vaid TP and Yap GPA. *Org. Lett.* 2006; **8**: 2401–2404.
5. Yamamoto Y, Hirata Y, Kodama M, Yamaguchi T, Matsukawa S, Akiba K, Hashizume D, Iwasaki F, Muranaka A, Uchiyama M, Chen P, Kadish KM and Kobayashi N. *J. Am. Chem. Soc.* 2010; **132**: 12627–12638.
6. Kakui T, Sugawara S, Hirata Y, Kojima S and Yamamoto Y. *Chem. —Eur. J.* 2011; **17**: 7768–7771.
7. Sugawara S, Kodama M, Hirata Y, Kojima S and Yamamoto Y. *J. Porphyrins Phthalocyanines* 2011; **15**: 1326–1334.
8. Hiramatsu S, Sugawara S, Kojima S and Yamamoto Y. *J. Porphyrins Phthalocyanines* 2013; **17**: 1183–1187.
9. Closs GL and Closs LE. *J. Am. Chem. Soc.* 1963; **85**: 818–819.
10. Buchler JW and Puppe L. *Liebigs Ann. Chem*. 1970; **740**: 142–163.
11. Sinyakov GN, Shul'ga AM, Filatov IV and Gurinovich GV. *Teor. Eksp. Khim.* 1988; **24**: 37–44.
12. Cosmo R, Kautz C, Meerholz K, Heinze J and Müllen K. *Angew. Chem., Int. Ed. Engl.* 1989; **28**, 604–607.
13. Yoshida T, Zhou W, Furuyama T, Leznoff DB and Kobayashi N. *J. Am. Chem. Soc*. 2015; **137**: 9258–9261.
14. Satoh T, Minoura M, Nakano H, Furukawa K and Matano Y. *Angew. Chem., Int. Ed.* 2016; **55**: 2235–2238.
15. Sudoh K, Satoh T, Amaya T, Furukawa K, Minoura M, Nakano H and Matano Y. *Chem. —Eur. J.* 2017; **23**: 16364–16373.
16. Sakida T, Yamaguchi S and Shinokubo H. *Angew. Chem., Int. Ed.* 2011; **50**: 2280–2283.
17. Matano Y, Shibano T, Nakano H and Imahori H. *Chem. —Eur. J*. 2012; **18**: 6208–6216.
18. Matano Y, Shibano T, Nakano H, Kimura Y and Imahori H. *Inorg. Chem.* 2012; **51**: 12879–12890.
19. Senge MO and Feng X. *J. Chem. Soc., Perkin Trans.* 1 **2000**; 3615–3621.
20. Krishnan R, Binkley JS, Seeger R and Pople JA. *J. Chem. Phys.* 1980; **72**: 650–654.
21. (a) Wachters AJH. *J. Chem. Phys.* 1970; **52**: 1033–1036. (b) Hay PJ. *J. Chem. Phys.* 1977; **66**: 4377–4384. (c) Raghavachari K and Trucks GW. *J. Chem. Phys.* 1989; **91**: 1062–1065.
22. (a) Becke AD. *J. Chem. Phys.* 1993; **98**: 5648–5652. (b) Lee C, Yang W and Parr RG. *Phys. Rev. B* 1988; **37**: 785–789.
23. Frisch MJ, Trucks GW, Schlegel HB, Scuseria GE, Robb MA, Cheeseman JR, Scalmani G, Barone V, Mennucci B, Petersson GA, Nakatsuji H, Caricato M, Li X, Hratchian HP, Izmaylov AF, Bloino J, Zheng G, Sonnenberg JL, Hada M, Ehara M, Toyota K, Fukuda R, Hasegawa J, Ishida M, Nakajima T, Honda Y, Kitao O, Nakai H, Vreven T, Montgomery, Jr. JA, Peralta JE, Ogliaro F, Bearpark M, Heyd JJ, Brothers E, Kudin KN, Staroverov VN, Keith T, Kobayashi R, Normand J, Raghavachari K, Rendell A, Burant JC, Iyengar SS, Tomasi J, Cossi M, Rega N, Millam JM, Klene M, Knox JE, Cross JB, Bakken V, Adamo C, Jaramillo J, Gomperts R, Stratmann RE, Yazyev O, Austin AJ, Cammi R, Pomelli C, Ochterski JW, Martin RL, Morokuma K, Zakrzewski VG, Voth GA, Salvador P, Dannenberg JJ, Dapprich S, Daniels AD, Farkas O, Foresman JB, Ortiz JV, Cioslowski J and Fox, DJ. *Gaussian 09, Revision B.01*; Gaussian, Inc., Wallingford CT, **2010**.
24. Stoll S and Schweiger A. *J. Magn. Reson*. 2006; **178**: 42–55.